Astronomical and Astrophysical Transactions (*AApTr*), 2012, Vol. 27, Issue 2, pp. 389–398,
ISSN 1055-6796, Photocopying permitted by license only, ©Cambridge Scientific Publishers

Modelling of the galactic kinematics

A.M. Mel'nik[1*], P. Rautiainen[2†]

[1] *Sternberg Astronomical Institute, Lomonosov Moscow State University, 13, Universitetskij pr., Moscow 119899, Russia*
[2] *Department of Physics/Astronomy Division, University of Oulu, P.O. Box 3000, FIN-90014 Oulun yliopisto, Finland*

Received 1 February, 2012

We present models (test particle simulations with analytical bars and N-body simulations) which reproduce the kinematics of OB-associations in the Perseus and Sagittarius regions. The directions of the radial and azimuthal components of the residual velocities can be explained by the presence of the outer pseudoring of class R_1R_2' in the Galaxy. The optimal value of the solar position angle with respect to the bar major axis providing the best agreement between the model and observed velocities is $\theta_b = 45 \pm 5^\circ$. The kinematics of the outer rings and pseudorings is determined by two processes: the resonance tuning and the gas outflow. The resonance kinematics is clearly observed in the pure rings, while the kinematics of the gas outflow is manifested itself in the pseudorings. N-body models can also reproduce kinematics in the Local System in addition to the Perseus and Sagittarius regions.

Keywords: Galaxy (Milky Way); Spiral structure; Kinematics and dynamics; Resonances

1 Introduction

There is a lot of evidence that our Galaxy includes the bar. The position angle of the bar is thought to be in the range $\theta_b = 15$–45°, in such a way that the end of the bar closest to the Sun lies in the first quadrant. The angular speed, hereafter pattern speed, of the bar, Ω_b, is not well known. Some researchers believe that the corotation radius (CR) lies at the distance $R_{CR} = 3$–4 kpc from the Galactic Center ([1, 2] and references therein), whereas others suggest that the Galaxy has a longer bar with $R_{CR} = 4$–5 kpc ([3–5] and references therein). In the case of flat rotation curve, the position of the CR of the bar in the interval $R_{CR} = 3$–5 kpc corresponds to the angular speed in the range $\Omega_b = 40$–70 km s^{-1} kpc^{-1} and to the position of the Outer Lindblad Resonance (OLR) in the solar vicinity $|R_{OLR} - R_0| < 1$ kpc.

The investigation of the Perseus region in OB-associations, red supergiants, molecular and neutral hydrogen showed the presence of systematical non-circular motions which were interpreted as motions directed towards the Galactic center [6–8]. Recent

*Email: anna@sai.msu.ru
†Email: pertti.rautiainen@oulu.fi

studies agree with this result [9–11]. The specific kinematics of the Perseus region can be explained by the presence of the spiral pattern situated within its CR. In such case, the pattern speed of the spiral Ω_{sp} must be lower than the speed due to rotation curve at the distance of the Perseus region ($R = 8.4$ kpc), i.e. $\Omega_{sp} < 25$ km s^{-1} kpc^{-1}. The angular speed of the spiral pattern supposed by [12], $\Omega_{sp} = 13$ km s^{-1} kpc^{-1}, can reproduce the systematical motions in the Perseus region [13].

Thus, the Galaxy would include at least two patterns (modes) rotating with different pattern speeds: the central region dominated by the bar rotating with $\Omega_b \approx 50$ km s^{-1} while the periphery would be dominated by the slowly rotating spiral with $\Omega_{sp} = 10$–25 km s^{-1}. Indeed, there are N-body models which include the bar and slow modes rotating on the periphery [14–17]. These models were not constructed to model any specific galaxy, but may be helpful in explaining the kinematical characteristics of the Galaxy.

However, even a simpler model of the Galaxy with the outer ring of class R_1R_2' can explain the kinematics of the Perseus region without invoking slow modes [18, 19]. The essential characteristic of the galaxies with the outer rings and pseudorings – broken rings – is the presence of the bar [20, 21]. Two main classes of the outer rings and pseudorings have been identified: the R_1 rings (R_1' pseudorings) elongated perpendicular to the bar and the R_2 rings (R_2' pseudorings) elongated parallel to the bar. In addition, there is a combined morphological type R_1R_2' which shows elements of both classes.

The test particle simulations [16, 22, 23] and N-body simulations [17] show that the outer pseudorings are typically located in the region of the Outer Lindblad Resonance (OLR). Schwarz [22] connected two main types of the outer rings with two main families of periodic orbits existing near the OLR of the bar [24, 25].

We constructed two different types of models which reproduce the kinematics of young stars in some stellar-gas complexes in the 3-kpc solar neighborhood. As will be shown below, the kinematics of young stars in the Perseus region indicates the existence of the R_2 ring, while the velocities in the Sagittarius region suggest the presence of the R_1 ring in the Galaxy. Good examples of R_1R_2' morphology are ESO 509-98 and ESO 507-16 [26], which could also be regarded as possible prototypes of the Galaxy.

2 Models with analytical bars

We consider motion of massless particles in an analytical potential. Our models have practically flat rotation curves and consist of bulge, bar, and halo. The bulge is modelled as a Plummer sphere, halo is an isothermal sphere, the bar is modelled as a Ferrers ellipsoid [27, 28]. We are making two-dimensional simulations without self-gravity. The gravitational effects of the rings and spiral arms are omitted in this stage of study. The gas subsystem is modelled by 50 000 massless particles that can collide with each other inelastically. Our models have nearly flat rotation curves (for more details, see [18]).

We compare the observed velocities of OB-associations in the stellar-gas complexes with the model velocities of gas particles which appeared to lie within the boundaries of stellar-gas complexes at certain moments. The Sagittarius region ($R = 5.6$ kpc) is

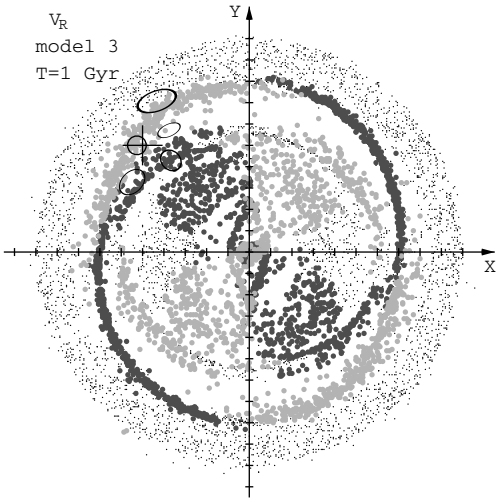


Figure 1 The distribution of particles (gas+OB) with the negative and positive radial residual velocities V_R at the moment $T = 1$ Myr. Particles with the positive V_R ($V_R > 5$ km s^{-1}) are indicated by black circles, while particles with the negative one ($V_R < -5$ km s^{-1}) – by grey circles. Particles with the velocities close to zero ($-5 < V_R < +5$ km s^{-1}) are shown by points. Only 20% of particles are shown. The bar is oriented along the Y-axis, the galaxy rotates clockwise, a division on the X- and Y-axis corresponds to 1 kpc. It also includes the boundaries of the stellar-gas complexes. The position of the sun is indicated by a cross.

the closest to the Galactic center, the Carina ($R = 6.5$ kpc) and Cygnus ($R = 6.9$ kpc) regions are located farther away, then goes the Local System ($R = 7.4$ kpc), and the outermost is the Perseus region ($R = 8.4$ kpc). To study the systematical motions we consider the residual velocities which are calculated as differences between the model velocities and the velocities due to the rotation curve.

Figure 1 exhibits the distribution of particles with positive and negative radial residual velocities V_R directed along the galactic radius-vector. The main kinematical feature of the pure rings is the alternation of the quadrants with the negative and positive residual velocities. Besides, particles located at the same azimuthal angle but forming either the R_1 or the R_2 ring have the opposite residual velocities. The resonance between the epicyclic and orbital motions adjusts the epicyclic motions of gas clouds in accordance with orbital rotation. This creates systematical non-circular motions of gas clouds whose direction depends on the position angle of a point with respect to the bar major axis and on the class of the outer ring. Figure 2 shows the directions of the residual velocities at the different points of the outer pseudorings. The directions of the residual velocities in our models at the moment $T = 1$ Gyr (Fig. 1) are in a good agreement with the resonance kinematics shown in Fig. 2. Probably, the kinematics of the pure rings is determined by the resonant orbits only.

Schwarz [22] finds that the gas outflow from the region close to the CR of the bar to the galactic periphery plays an important role in the formation of the outer rings. Figure 3 shows the distribution of gas particles along the galactic radius R

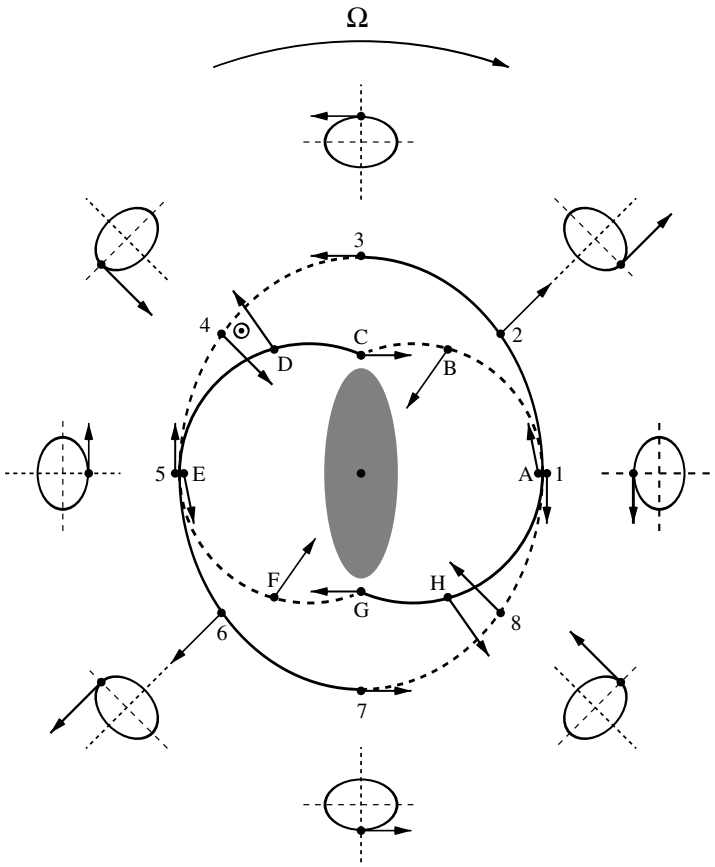


Figure 2 Orbital kinematics in the resonance region. The bar and two main families of periodic orbits in the region of the OLR are shown. The galaxy rotates clockwise. Motions are considered in the reference frame rotating with the speed of the bar. The orbit going through the points 1-2-3-4-5-6-7-8 represents the family of periodic orbits elongated along the bar. This family is the backbone of the R_2 ring. The orbit A-B-C-D-E-F-G-H denotes the family of periodic orbits elongated perpendicular to the bar which are forming the R_1 ring. The epicycles drawing on the border of the picture show the position of a particle on the epicyclic orbit at the points 1–8. The vectors show the directions of the additional (residual) velocities due to the epicyclic motion. The dashed lines indicate the orbital segments with the negative radial velocity, while the solid lines – those with the positive velocity V_R. The likely position of the Sun is shown by the specific symbol.

at different moments. At the initial moment the surface density is constant in the interval $R = 1$–10 kpc in all models. At the moment $T = 1$ Gyr the density profiles have a well-defined maximum corresponding to the location of the R_2 ring ($R = 7$–8 kpc). In all models the maximum corresponding to the R_1 ring is lying clearly inside the OLR, in the vicinity of the outer 4/1 resonance, while the maximum corresponding to the R_2 ring is shifted ~ 0.5 kpc outside the OLR.

We found that the kinematics of the outer rings and pseudorings is determined

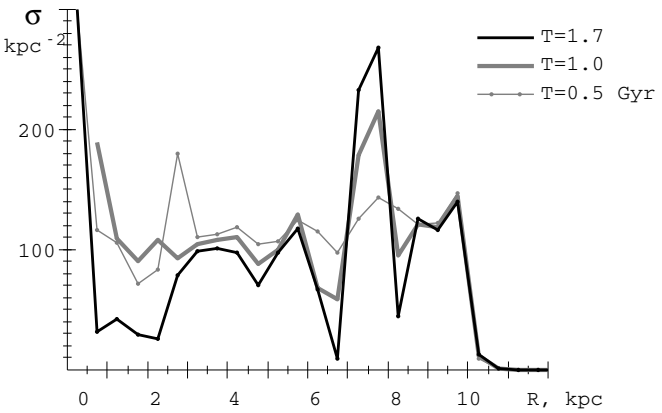


Figure 3 Gas-density profiles made for 3 different moments. A well-defined maximum corresponding to the location of the R_2 ring.

by two processes: the resonance tuning and the gas outflow. Models of the Galaxy with the R_1R_2' pseudoring reproduce well the radial and azimuthal components of the residual velocities in the Perseus and Sagittarius regions: the difference between the model and observed velocities does not exceed 3 km s^{-1}.

3 N-body simulations

We also made several N-body models, which satisfy a broadly defined set of observational constraints: the rotation curve is essentially flat and the size of the bar is acceptable. From these models we have chosen our best-fitting case, which is described here. We scaled the simulation units to correspond to our preferred values of the solar distance from the Galactic center and the local circular velocity. This also gives the scales for masses and time units. The galactic disk in our model includes two subsystems. The stellar subsystem is modelled by 8 million self-gravitating collisionless particles while the gas subsystem is modelled by 40 000 massless particles which can collide with each other inelastically. The bulge and halo components are analytical. The N-body models are two-dimensional, the value of the gravitation softening is $\sim$ 0.2 kpc, with the adopted length scale. The mass of the disk $M_{disk} = 3.51 \times 10^{10}\ M_{\odot}$. The stellar disk quickly forms a bar. Its original pattern speed is quite high meaning that when it forms, it does not have an Inner Lindblad Resonance. In the beginning, the bar slows down quite quickly, then its pattern speed almost stabilizes and the length of the bar amounts $R_{bar} = 4$ kpc. The bar can always be considered dynamically fast [29]. There is no secondary bar in this model. The gas disk forms an outer ring which exhibits elements of R_1- and R_2-morphology and can be often classified as R_1R_2 ring. Note that there is no evolutionary trend between the morphological stages, they all appear and disappear several times (for more details, see [19]).

Figure 4 exhibits the amplitude spectra of the relative density perturbations in the model stellar disk (see e.g. [15, 16]). We can see that the bar mode is not the

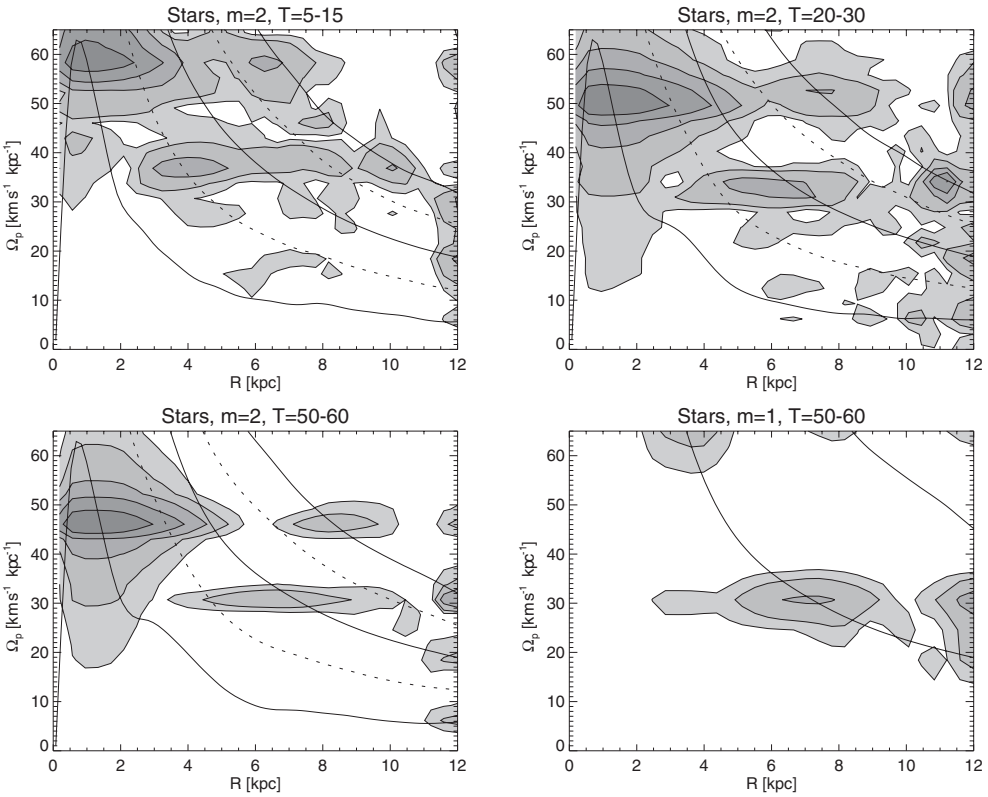


Figure 4 The amplitude spectra of the relative density perturbations in the model disk. The frames show the amplitude spectra of the stellar component at various times (indicated on the frame titles). The contour levels are 0.025, 0.05, 0.1, 0.2, 0.4, and 0.8, calculated with respect to the azimuthal average surface density at each radius. The continuous lines show the frequencies Ω and $\Omega \pm \kappa/m$, and the dashed curves indicate the frequencies $\Omega \pm \kappa/4$ in the $m = 2$ amplitude spectrum.

only one in the disk, but there are also slower modes. The bar mode rotates with the speed of 47 km s^{-1} kpc^{-1} but the strongest slow mode with the speed of 31 km s^{-1} kpc^{-1}. We have also tried to reconstruct the shapes of the modes. This was done by averaging the surface density in the reference frames co-rotating with the modes. No assumptions were made about the shapes of the modes (Fig. 5). We can see that the bar mode includes the bar and symmetrical spiral structure that forms an R_1 outer ring. In some galaxies with the combined R_1R_2'-morphology the R_1-rings can be seen also in the near infrared [23]. N-body simulations also confirm that the R_1'-rings can be forming in the self-gravitating stellar subsystem. On the other hand, the strongest slow mode is clearly lopsided. Interestingly, there is an overlap of resonances with the bar modes: the corotation of the bar coincides with the inner 4/1 resonance of the slow mode. The same resonance overlap was common in the models of Rautiainen & Salo [16], and has been also reported by Debattista et al. [30].

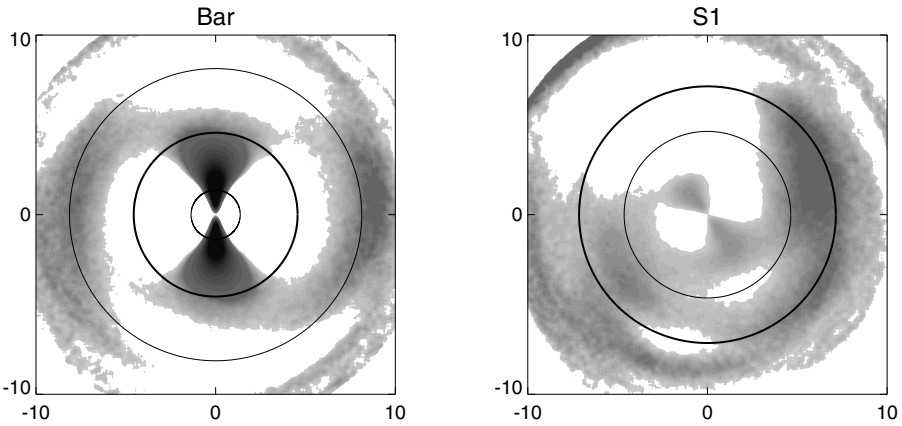


Figure 5 The reconstructed modes in the stellar component for $T = 5$–6 Myr interval. The enhanced density compared to the azimuthally averaged profile at each radius is shown. The shades of gray (darker corresponds to higher surface density) have been chosen to emphasize the features. The circles in the bar mode indicate ILR (1.4 kpc), CR (4.6 kpc), and OLR (8.1 kpc), whereas the inner 4/1 (4.6 kpc) and CR (7.1 kpc) are shown for the mode S1.

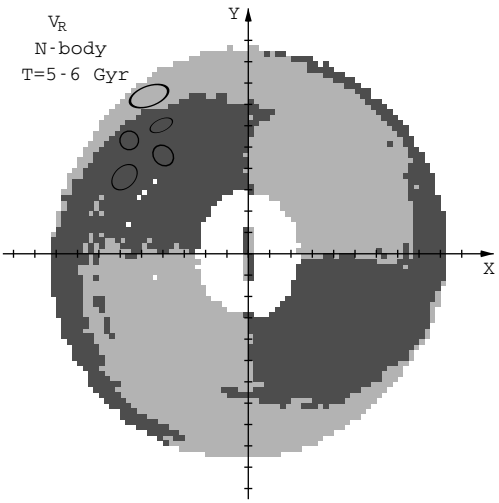


Figure 6 Distribution of the negative and positive average residual velocities V_R calculated in squares. The squares with positive V_R are shown in black, while those with negative ones are given in gray. Only squares that have enough number of particles are depicted. It also demonstrates the boundaries of the stellar-gas complexes. The position angle of the Sun is supposed to be $\theta_b = 45^\circ$. The bar is oriented along the Y-axis, the galaxy rotates clockwise, and a division on the X- and Y-axis corresponds to 1 kpc.

For each stellar-gas complex we calculated its momentary and average velocities. We selected gas particles located within the boundaries of the stellar gas complexes

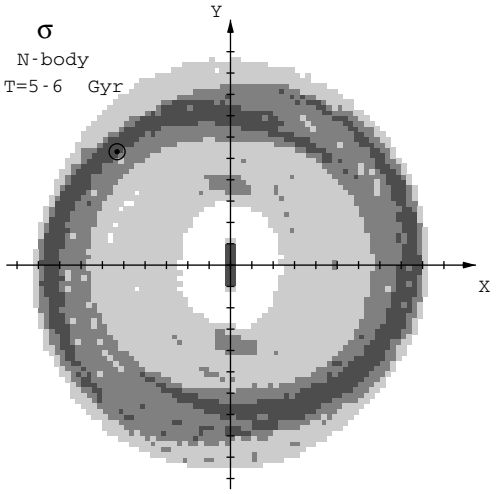


Figure 7 The surface density of gas particles averaged in squares at the time interval $T = 5$–6 Gyr. The light-gray, dark-gray, and black colors represent squares containing the increasing number of particles. The position of the Sun is shown by the specific symbol. The bar is oriented along the Y-axis, the galaxy rotates clockwise, and a division on the X- and Y-axis corresponds to 1 kpc.

and calculated their mean velocities for each moment. The momentary velocities of stellar-gas complexes oscillate near their average values within the limits of $\sim \pm 20$ km s^{-1}. Two processes are probably responsible for these oscillations. The first is the slow modes that cause quasi-periodic velocity variations. The second process is likely connected with the short-lived perturbations, e.g. from transient spiral waves in the stellar component [31]. The averaging of velocities over long time interval reduces the influence of slow modes and occasional perturbations.

Figure 6 demonstrates the distribution of the average velocities on the galactic plane. We divided the area ($-10 < x < +10$, $-10 < y < +10$ kpc) into small squares of a size 0.250×0.250 kpc and calculated the average residual velocities in small squares over large time interval (1 Gyr). The distribution of the negative and positive velocities obtained for N-body simulations strongly resembles that of the pseudorings in models with analytical bars, giving support to the "averaging process" adopted here.

Figure 7 shows the surface density of gas particles averaged in squares over 1 Gyr. This was done by averaging the surface density in the reference frame co-rotating with the bar. We can see that the density perturbation inside the outer ring can be approximated by two tightly wound spiral arms whose pitch angle is about $i = 6 \pm 1°$.

4 Conclusions

Our N-body models reproduce the observed residual velocities in the Perseus and Sagittarius regions and in the Local System. The mean difference between the model

and observed velocities is $\Delta v = 3$ km s^{-1} there. The optimal value of the solar position angle providing the best agreement between the model and observed velocities is $\theta_b = 45°$.

The models with analytical bars also reproduce well the observed velocities in the Perseus and Sagittarius regions. We explain this success by the resonance between the orbital rotation and the epicyclic motion. However, models with analytical bar failed dramatically with the Local System where they yielded only negative radial velocities whereas the observed value is positive. The success of N-body simulations with the Local System is likely due to the gravity of the stellar R_1-ring, which is omitted in models with analytical bars.

Acknowledgements

We wish to thank Heikki Salo for using his simulation code [32, 33]. This work was partly supported by the Russian Foundation for Basic Research (project no. 10-02-00489).

References

[1] Englmaier, P. and Gerhard, O. (2006) *Celest. Mechan. Dynamic. Astron.* **94**, 369.
[2] Habing, H.J., Sevenster, M.N., Messineo, M. et al. (2006) *Astron. Astrophys.* **458**, 151.
[3] Weiner, B.J. and Sellwood, J.A. (1999) *Astrophys. J.* **524**, 112.
[4] Benjamin, R.A., Churchwell, E., Babler, B.L. et al. (2005) *Astrophys. J.* **630**, L149.
[5] Cabrera-Lavers, A., Hammersley, P.L., Gonzalez-Fernandez, C. et al. (2007) *Astron. Astrophys.* **465**, 825.
[6] Burton, W.B. and Bania, T.M. (1974) *Astron. Astrophys.* **33**, 425.
[7] Humphreys, R.M. (1976) *Astrophys. J.* **206**, 114.
[8] Brand, J. and Blitz, L. (1993) *Astron. Astrophys.* **275**, 67.
[9] Mel'nik, A.M., Dambis, A.K., Rastorguev, A.S. (2001) *Astron. Lett.* **27**, 521.
[10] Sitnik, T.G. (2003) *Astron. Lett.* **29**, 311.
[11] Mel'nik, A.M. and Dambis, A.K. (2009) *Mon. Not. R. Astron. Soc.* **400**, 518.
[12] Lin, C.C. (1970) *The Spiral Structure of our Galaxy*, IAU Symp. No 38, Ed. by W. Becker and G. Contopoulos (Reidel, Dordrecht) p. 377.
[13] Roberts, W.W. (1972) *Astrophys. J.* **173**, 259.
[14] Sellwood, J.A. and Sparke, L.S. (1988) *Mon. Not. R. Astron. Soc.* **231**, 25.
[15] Masset, F. and Tagger, M. (1997) *Astron. Astrophys.* **322**, 442.
[16] Rautiainen, P. and Salo, H. (1999) *Astron. Astrophys.* **348**, 737.
[17] Rautiainen, P. and Salo, H. (2000) *Astron. Astrophys.* **362**, 465.
[18] Mel'nik, A.M. and Rautiainen, P. (2009) *Astron. Lett.* **35**, 609.
[19] Rautiainen, P. and Mel'nik, A.M. (2010) *Astron. Astrophys.* **519**, 70.
[20] Buta, R. (1995) *Astrophys. J. Suppl. Ser.* **96**, 39.
[21] Buta, R. and Combes, F. (1996) *Fund. Cosmic Physics* **17**, 95.
[22] Schwarz, M.P. (1981) *Astrophys. J.* **247**, 77.

[23] Byrd, G., Rautiainen, P., Salo, H., Buta, R., Crocker, D.A. (1994) *Astrophys. J.* **108**, 476.
[24] Contopoulos, G. and Papayannopoulos, Th. (1980) *Astron. Astrophys.* **92**, 33.
[25] Contopoulos, G. and Grosbol, P. (1989) *Astron. Astrophys. Review* **1**, 261.
[26] Buta, R., Crocker, D.A. (1991) *Astron. J.* **102**, 1715.
[27] Athanassoula, E. (1992) *Mon. Not. R. Astron. Soc.* **259**, 328.
[28] Romero-Gómez, M., Athanassoula, E., Masdemont, J.J. et al. (2007) *Astron. Astrophys.* **472**, 63.
[29] Debattista, V.P. and Sellwood, J.A. (2000) *Astrophys. J.* **543**, 704.
[30] Debattista, V.P., Mayer, L., Carollo, C.M., Moore, B., Wadsley, J., Quinn, T. (2006) *Astrophys. J.* **645**, 209.
[31] Sellwood, J.A. (2000) *Astrophys. and Space Science* **272**, 31.
[32] Salo H. (1991) Astron. Astrophys. **243**, 118.
[33] Salo H. and Laurikainen E. (2000) *Mon. Not. R. Astron. Soc.* **319**, 377.